Molecular Characterization of Organosulfur Compounds in Biodiesel and Diesel Fuel Secondary Organic Aerosol

Sandra L. Blair,[†] Amanda C. MacMillan,[†] Greg T. Drozd,[‡] Allen H. Goldstein,[‡] Rosalie K. Chu,[§] Ljiljana Paša-Tolić,[§] Jared B. Shaw,[§] Nikola Tolić,[§] Peng Lin,[§] Julia Laskin,[‖] Alexander Laskin,[§] Sergey A. Nizkorodov[†*]

[†]Department of Chemistry, University of California, Irvine, Irvine, CA 92697, USA
[‡]Department of Environmental Science, Policy, & Management, University of California, Berkeley, Berkeley, CA 94720, USA
[§]Environmental Molecular Sciences Laboratory and [‖]Physical Sciences Division, Pacific Northwest National Laboratory, Richland, WA 99354, USA

Contents

Fuel Analysis

Samples were diluted (100:1) in chloroform (Sigma-Aldrich, HPLC grade). The diluted samples were directly injected into a liquid nitrogen cooled inlet for cryo-focusing on a quartz wool inlet liner (CIS4, Gerstel, Inc.) at –25 °C. Injection into the GC column was achieved by rapid heating of the liner (10 °C s^{-1}) up to 320 °C under a flow of helium. Analytes were separated using an Agilent 7890 GC equipped with a non-polar primary column (60 m × 0.25 mm × 250 μm Rxi-5Sil-MS, Restek) and a secondary column (1 m Rtx-200, Restek) using a flow rate of 2 mL min^{-1} helium. The GC temperature program was as follows: 40 °C with 5 min hold, 3.5 °C min^{-1} up to 320 °C, and a final hold at 320 °C for 10 min. Following GC separation, analytes were ionized using standard electron impact ionization (EI) and a vacuum-ultraviolet (VUV) photon beam at 10.5 eV. Analytes were detected using a time-of-flight (ToF) mass spectrometer (TOFWERK) operated in positive mode with a resolving power of $m/\Delta m \approx 4000$. Data were collected at 100 Hz and signal averaged to 0.5 Hz. The ion source was operated at the reduced temperature of 170 °C to minimize fragmentation with VUV ionization and 270 °C with EI ionization to better maintain volatilization of the GC effluent. The VUV photon flux of ~10^{16} photons cm^{-2}·s was generated by the Chemical Dynamics Beamline 9.0.2 of the Advanced Light Source at Lawrence Berkeley National Laboratory.

Our calibration methods are based on the method used in Worton et al. 2015,[1] Isaacman et al. 2012,[2] and Chan et al. 2013.[3] The molecular ion signals for linear, branched, cyclic, and aromatic hydrocarbons under VUV ionization are used as the basis for quantification. Sensitivity of the molecular ion for any given compound is a function of its thermal transfer efficiency, ionization efficiency, and degree of fragmentation. For molecules with a given carbon number, the molecular ion signal increases with increasing number of double bond equivalency (NDBE) because of reduced fragmentation. Authentic standards of more than 80 compounds were used for calibration; these included n-alkanes, branched alkanes, n-alkyl cyclohexanes, n-alkyl benzenes, hopanes, steranes, PAHs, and alkylated PAHs. These species were selected to span both carbon number and NDBE ranges of the diesel samples. This yields NDBE-specific calibration curves for NDBE = 0, 1, 4, and 7+ due to limited availability of authentic standards for the other NDBE's. The previous work referenced has shown that intermediate NDBE sensitivities can be interpolated.

Thermal transfer efficiency is not linear with carbon number because early and late eluting components have lower efficiency for transfer than intermediate eluting components. A series of perdeuterated n-alkanes (even carbon numbers from C8-C34) was added as an internal standard to all samples to generate a relationship between thermal transfer and retention time.

Total analytical uncertainty includes contributions from transfer efficiency, structural differences in fragmentation within a NDBE class, and uncertainties in calibration curves. The uncertainty in calibrating response to mass, determined from calibration curves of authentic standards, was structurally and mass-dependent with larger uncertainties for lower NDBE species and smaller mass fractions. The total analytical uncertainty was < 40% for all species at mass fractions above 0.1%, increasing to < 70% at mass fractions below 0.01%. Blanks run without any sample injection showed that background levels were negligible compared with observed levels of analytes in the samples. Repeat analyses showed analytical precision was < 25% for each compound class.

The relative composition of the main components of the biodiesel was determined utilizing the similar sensitivity observed for standards of mono-unsaturated fatty acids in this carbon range (oleic, linoleic, palmitoleic) and accounting for thermal transfer efficiency as above that of the diesel #2 sample. The speciation of the biodiesel components was done using EI ionization and utilizing NIST library searches. All compounds identified had match factors above 850, most above 900.

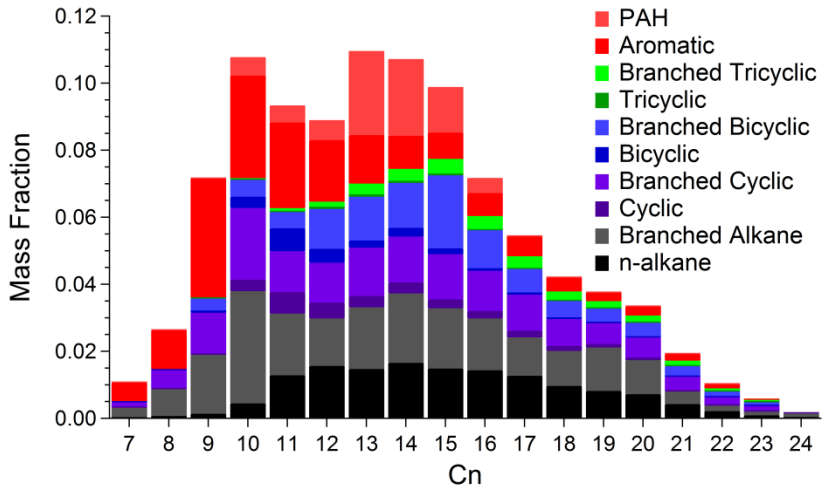

Figure S1. Mass fraction of species in diesel fuel from GC-VUV-MS analysis as a function of the carbon number (Cn) of detected molecules. Species are stacked in the bar graph such that the height of the combined bars for a specific Cn represents the mass fraction.

Additional Details on Chamber Generation of SOA

We kept the initial VOC mixing ratio as close as possible between different experiments by following the same injection procedure. High concentrations of precursors used in this study were necessary for the offline measurements of SOA absorption coefficients (to be reported in a future paper). A measured volume of H_2O_2 (Aldrich, 30 v/v % in water), used as the OH precursor, was added to the chamber by evaporation with a stream of zero air to achieve a final concentration of 2 ppm H_2O_2. Hydrogen peroxide was used as the OH precursor instead of the more common HONO so that low-NO_x experiments (future publication) can be more easily compared to the high-NO_x experiments. Then, NO (Praxair, 5000 ppm NO in N_2) and/or SO_2 (Airgas, 1000 ppm SO_2 in N_2) were introduced to the chamber from pre-mixed gas cylinders. NH_3 was introduced to the chamber from a 1:10 dilution of an ammonium hydroxide aqueous solution (Fisher, 14.8 N) and evaporated into the chamber with a stream of zero air. Despite extensive cleaning, we cannot rule out contamination by ammonia in experiments in which ammonia was not intentionally added because outgassing of ammonia from chamber walls is a common problem.[4] However, the ammonia mixing ratios used in our experiments (100 or 1000 ppb) was significantly higher than could be obtained from outgassing (for example, 5 ppb in a dry chamber and 35 ppb at 50% RH in Liu et al. 2015[4]). Solutions of diesel fuel and/or biodiesel

fuel in dichloromethane (we previously verified using HRMS methods that presence of CH_2Cl_2 in the chamber does not result in the production of chlorinated organics) were added in the same manner and the chamber content was mixed for several minutes using a Teflon^{TM}-coated fan.

Discussion of Likely SOA Precursors in the Fuels

Diesel fuel composition was much more complex than that of biodiesel fuel. Consistent with previous reports, diesel fuel was composed of 25% aromatics and 75% aliphatics with an average carbon number of 14 (Figure S1).[2] Though the mass distribution was not measured for compounds below 7 carbon atoms, these compounds are estimated to account for less than 1% of the total mass, consistent with previous analyses.[5] Polycyclic aromatic hydrocarbons (PAHs) in the diesel fuel were dominated by methylated naphthalenes, with 1 to 3 methyl groups. Photooxidation SOA yield generally decreased in previous studies in the order of aromatics > cycloalkanes > *n*-alkanes or multi-ring aromatics > branched alkanes.[6-7] All of these components, including the higher SOA yielding aromatic compounds, such as naphthalene (NAP), were observed in diesel fuel, confirming that this fuel sample should produce SOA with measurable yields.

The major known components of soy bean oil are linoleic acid (55%), oleic acid (18%), linolenic acid (10%), palmitic acid (10%), and stearic acid (4%).[8] The biodiesel used in this study consisted of primarily C_{19} (~85%) and C_{17} (~15%) FAMEs of the original fatty acids found in soy bean oil. Small amounts of C_{21} and C_{23} FAMEs were also observed. The most abundant FAMEs were methyl linoleate and methyl oleate, as expected from the predominance of linoleic and oleic acids in soy bean oil. Unsaturated FAMEs in biodiesel fuel such as methyl oleate, methyl linoleate, and methyl linolenate have one, two, and three double bonds, respectively, as reactive sites for OH or SO_2 addition, making biodiesel fuel more reactive than diesel fuel. However, the larger reactivity of biodiesel may be counteracted by the tendency of FAMEs to fragment, which reduced the SOA yields. Photooxidation of long-chain esters, such as the FAMEs in biodiesel fuel, has not been well studied, but FAMEs have been observed to preferentially fragment rather than just functionalize.[9-10]

An example of a time profile of SOA formation from diesel is plotted in Figure S2. Particles formed within minutes after photooxidation started, and then grew to a maximum mass concentration after 3 h, at which point the sampling of SOA started. Peak SOA mass concentrations and particle diameters are listed in Table 1. In general, addition of SO_2 increased SOA mass concentrations and particle diameters, whereas addition of NH_3 caused a minor decrease from the base case of 'no SO_2' present. The smaller observed SOA mass concentrations of the biodiesel SOA (BDSL SOA) samples (samples 6 and 7) are most likely due to the photochemical degradation of FAMEs to smaller gaseous species (although we cannot rule out incomplete oxidation or unaccounted losses of biodiesel fuel in the injection lines). The 20% biodiesel in diesel fuel mixture SOA (MIX SOA) experiments (samples 8 and 9) had SOA mass concentrations and particle diameters between the values of the diesel SOA (DSL SOA) and BDSL SOA samples (Table 1). Overall, all samples had similar particle mean geometric diameters except for the BDSL SOA samples, which grew to smaller sizes.

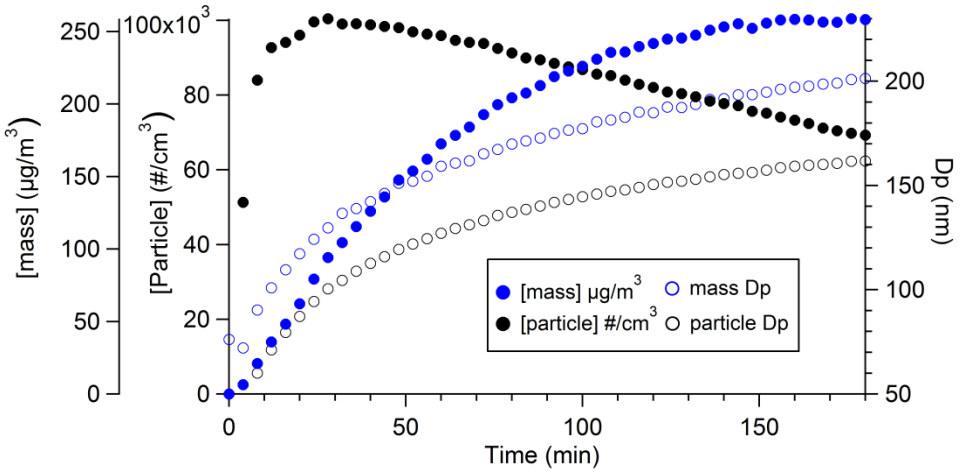

Figure S2. Sample SMPS data for SOA formation from sample 1 (DSL/NOx). Time zero corresponds to turning on the UV lamps. The SMPS and AMS sampled throughout the entire experiment. Sampling for high-resolution offline analysis started after ~3 h of photooxidation when the particle mass concentration reached the maximum.

Table S1. Average molecular formulas and ratios of SOA samples from nano-DESI/HRMS spectra. Data for samples also recorded with 21T FT-ICR-MS are provided in parentheses.

Sample	Sample Code	<C>	<H>	<O>	<N>	<S>	<DBE>
1	DSL/NO_x	10.46	12.34	6.56	0.38	–	5.48
2	DSL/NO_x/SO_2	11.84 (13.44)	20.57 (23.56)	7.28 (6.85)	0.67 (0.00)	0.91 (0.93)	2.88 (2.67)
3	DSL/NO_x/SO_2/NH_3	12.26	21.99	7.00	0.42	0.92	2.47
4	DSL/NO_x/RH	9.93	10.94	6.06	0.10	–	5.51
5	DSL/NO_x/SO_2/RH	12.15	14.91	5.66	0.16	0.23	5.77
6	BDSL/NO_x	10.22	13.45	6.48	0.14	–	4.57
7	BDSL/NO_x/SO_2	12.96 (12.49)	15.67 (19.35)	7.70 (7.69)	0.72 (0.16)	0.87 (0.89)	6.48 (3.89)
8	MIX/NO_x	9.11	11.08	5.88	0.37	–	4.76
9	MIX/NO_x/SO_2	15.25 (12.64)	20.46 (21.58)	7.52 (6.81)	0.75 (0.04)	0.78 (0.95)	6.40 (2.87)
10	DSL/NO_x[a]	11.77 (15.57)	16.54 (21.03)	4.92 (7.57)	0.03 (0.03)	–	4.52 (6.08)
11	DSL/NO_x/SO_2[a]	11.64 (11.74)	17.44 (20.91)	5.02 (6.84)	0.02 (0.02)	0.18 (97)	3.94 (2.29)
12	DSL/NO_x/SO_2-high[a]	10.85 (12.35)	18.08 (21.92)	5.91 (6.86)	0.06 (0.04)	0.57 (0.87)	2.84 (2.41)
13	DSL/NO_x/SO_2/NH_3[a]	10.32 (11.47)	18.88 (21.57)	5.59 (6.02)	0.10 (0.03)	0.85 (0.96)	1.93 (1.70)

[a]Samples sent through a longer denuder train before collection.

Nano-DESI/HRMS and 21T FT-ICR-MS Data Analysis and Processing

Mass spectral features with a minimum signal-to-noise ratio of 3 were extracted from the averaged mass spectra of both solvent background and sample using Decon 2LS software developed at PNNL (http://omics.pnl.gov/software/decontools-decon2ls). Peaks from the background and sample mass spectra were clustered and sample peaks less than 3 times larger than the background were removed. Formula assignments with constraints of *c*: 1–40, *h*: 2–80, *o*: 0–35, *n*: 0–1, *s*: 0–1, O/C or O*/C: 0–1.2, H/C: 0.3–2.25 were performed using the Molecular Formula Calculator (https://nationalmaglab.org/user-facilities/icr/icr-software) for ions of the type $[M–H]^-$ with a tolerance for nano-DESI/HRMS and 21T FT-ICR-MS of *m/z* 0.001 and 0.0005, respectively.

Carbon Number Distribution of Aromatic Compounds in Fuels and SOA

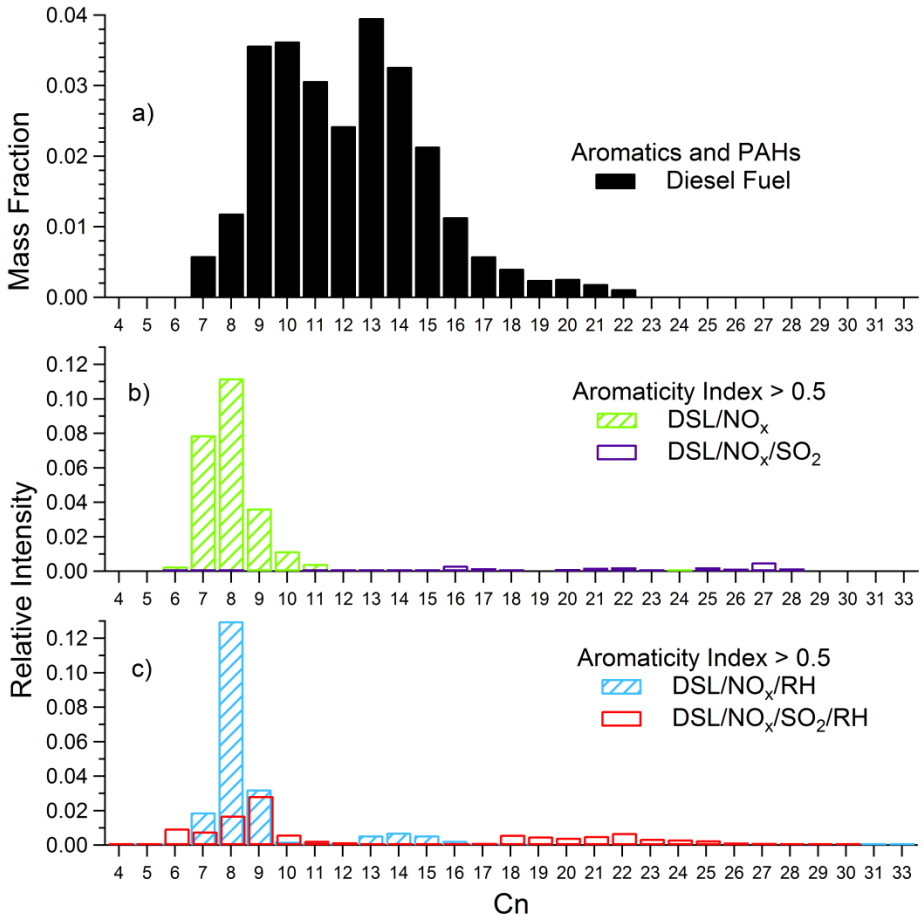

Figure S3. Comparison of aromatic species in diesel fuel and DSL SOA samples. Mass fraction of aromatics and PAHs of (a) diesel fuel and mass spectral relative intensities of (b) dry and (c) humid DSL SOA samples are overlaid in bar plots. Relative intensities of SOA samples were

normalized to fractions such that the sum of relative intensities of all of the peaks in an individual sample is 1; the relative intensities of mass spectral peaks of the same Cn were summed.

SOA from Photooxidation of BDSL/DSL Mixture

To explore how photooxidation of the diesel-biodiesel fuel mixture changed SOA composition, high-resolution mass spectra of SOA formed from the fuel mixture were decomposed into contributions from DSL SOA and BDSL SOA by analysis of the mass spectral patterns. Specifically, the FT-ICR MS mass spectrum of the MIX/NO_x/SO_2 sample was compared to those of the DSL/NO_x/SO_2 and BDSL/NO_x/SO_2 samples generated under similar experimental conditions. A least squares analysis of the intensities of individual peaks in the three samples was used to solve for coefficients "a" and "b" in eq S1, below.

$$MS_{\mathrm{MIX/NO}_x/\mathrm{SO}_2} = \mathrm{a} \cdot MS_{\mathrm{DSL/NO}_x/\mathrm{SO}_2} + \mathrm{b} \cdot MS_{\mathrm{BDSL/NO}_x/\mathrm{SO}_2} \quad \text{(S1)}$$

Only peaks in the individual samples that overlapped with MIX/NO_x/SO_2 were used in the fit analysis, but all peak intensities were later scaled by the coefficients and summed to represent a linear combination of mass spectra (Figure S4). Peak intensities were normalized such that the largest peak had a relative intensity (RI) of 100%. The intensity-weighted percent of the BDSL/NO_x/SO_2 mass spectrum in the calculated spectrum of the SOA produced from the mixture of fuels was 18%. This value is surprisingly close to the SOA fuel precursor composition of 20% biodiesel in diesel fuel. Several peaks observed in the individual fuel SOA samples were absent in the MIX SOA sample. In addition, several new peaks detected in the mixed SOA sample were not observed in spectra of the individual fuel SOA samples (Figure S5). A Venn diagram of peak overlap between mixed and individual SOA samples weighted by intensity is shown in Figure S6, where areas are proportional to the number of peaks. The largest peak in the BDSL/NO_x/SO_2 sample vanished in the mixed sample, $C_8H_{18}O_8S$ (100% RI), whereas the rest of the peaks lost were less than 20% RI. The DSL/NO_x/SO_2 peaks lost in the mixed sample were 10% RI or less. Although new peaks observed in MIX/NO_x/SO_2 only contributed 3% to the overall intensity of the mass spectrum, they amounted to 65 peaks. The percent CHO, CHON, CHOS, and CHONS of the new peaks, weighted by intensity, were 5%, 3%, 20%, and 72%, respectively. Under high-NO_x conditions used in this experiment, cross-reactions between alkyl peroxy radicals in diesel fuel and biodiesel fuel SOA are highly unlikely to occur in the gas-phase. The new and lost peaks in the organic composition of MIX/NO_x/SO_2 are most likely attributed to condensed-phase or heterogeneous reactions following particle formation.

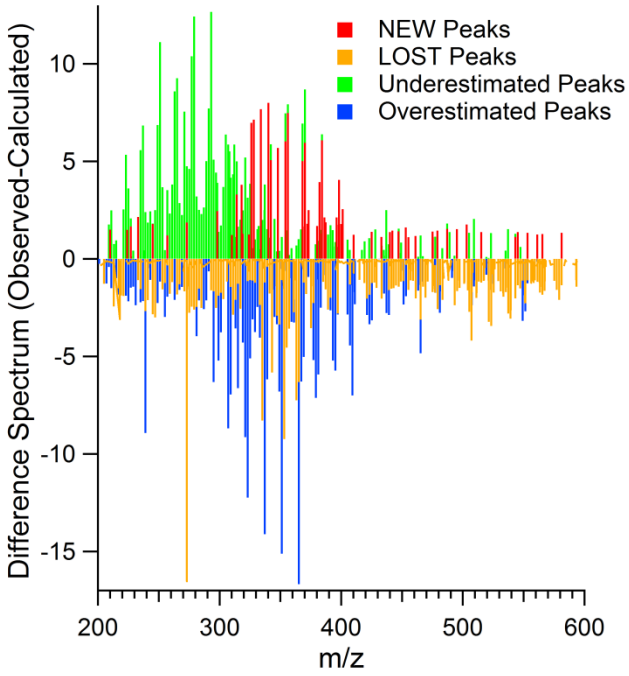

Figure S4. The difference 21T FT-ICR-MS spectra between observed and calculated MIX/NOx/SO_2. New and lost peaks of individual samples relative to the observed sample are also plotted. Note the change in scale relative to Figure S6.

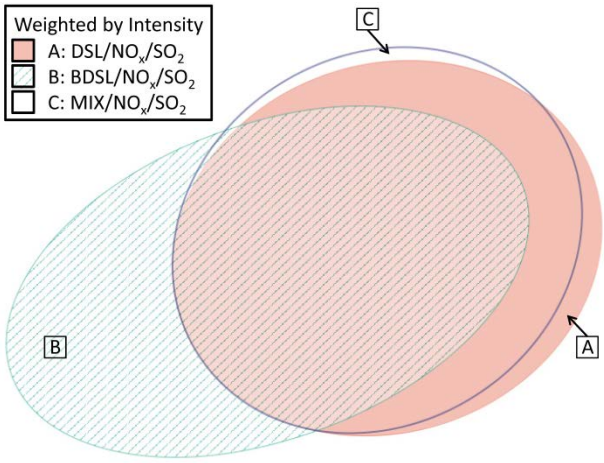

Figure S5. A Venn diagram of the overlap of 21T FT-ICR-MS peaks between DSL/NOx/SO_2 (A), BDSL/NOx/SO_2 (B), and MIX/NOx/SO_2 (C) weighted by peak intensities. Ellipsoid overlap represents peaks in common between samples; area overlap is weighted by the intensities of peaks in common between samples.

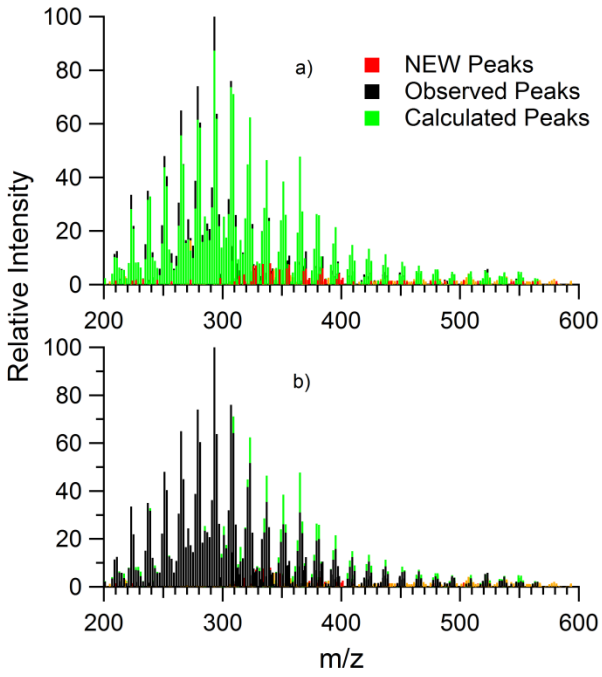

Figure S6. 21T FT-ICR-MS spectra of observed peaks and new peaks in MIX/NOx/SO_2 and a calculated spectrum of a linear combination of DSL/NOx/SO_2 and BDSL/NOx/SO_2 fit to overlapping peaks with the MIX/NOx/SO_2 sample. Mass spectra are displayed as a) calculated peaks overlaid with observed peaks and b) observed peaks overlaid with calculated peaks.

Table S2. Average atomic ratios of SOA samples from nano-DESI/HRMS and AMS data. Data for samples also recorded with 21T FT-ICR-MS are provided in parentheses.

Sample #	Sample Code	HRMS		AMS	
		<O/C>	<H/C>	<O/C>	<H/C>
1	DSL/NO_x	0.66	1.13	0.45	1.64
2	DSL/NO_x/SO_2	0.71 (0.53)	1.82 (1.75)	0.43	1.67
3	DSL/NO_x/SO_2/NH_3	0.63	1.83	0.41	1.69
4	DSL/NO_x/RH	0.66	1.11	0.45	1.67
5	DSL/NO_x/SO_2/RH	0.55	1.25	0.46	1.7
6	BDSL/NO_x	0.67	1.3	0.49	1.69
7	BDSL/NO_x/SO_2	0.77 (0.74)	1.33 (1.69)	0.51	1.58
8	MIX/NO_x	0.67	1.2	0.46	1.68
9	MIX/NO_x/SO_2	0.59 (0.56)	1.52 (1.72)	0.43	1.69
10	DSL/NO_x[a]	0.44 (0.51)	1.39 (1.35)	0.44	1.7
11	DSL/NO_x/SO_2[a]	0.46 (0.61)	1.48 (1.78)	0.43	1.73
12	DSL/NO_x/SO_2-high[a]	0.58 (0.59)	1.67 (1.78)	0.43	1.71
13	DSL/NO_x/SO_2/NH_3[a]	0.61 (0.55)	1.85 (1.88)	0.42	1.72

[a]Samples sent through a longer denuder train before collection.

Table S3. Composition of species in SOA samples from nano-DESI/HRMS spectra. Data for samples also recorded with 21T FT-ICR-MS are provided in parentheses.

Sample #	Sample Code	% CHO	% CHON	% CHOS	% CHONS
1	DSL/NO_x	67	33	–	–
2	DSL/NO_x/SO_2	2 (8)	8 (0)	47 (92)	43 (0)
3	DSL/NO_x/SO_2/NH_3	5	5	59	31
4	DSL/NO_x/RH	91	9	–	–
5	DSL/NO_x/SO_2/RH	71	7	17	5
6	BDSL/NO_x	87	13	–	–
7	BDSL/NO_x/SO_2	17 (4)	11 (8)	44 (80)	28 (8)
8	MIX/NO_x	77	23		
9	MIX/NO_x/SO_2	10 (4)	16 (8)	34 (80)	40 (8)
10	DSL/NO_x[a]	97 (96)	3 (4)	–	–
11	DSL/NO_x/SO_2[a]	81 (3)	1 (0)	17 (95)	1 (2)
12	DSL/NO_x/SO_2-high[a]	43 (3)	0 (0)	51 (94)	6 (3)
13	DSL/NO_x/SO_2/NH_3[a]	11 (3)	5 (0)	81 (93)	3 (3)

[a]Samples sent through a longer denuder train before collection.

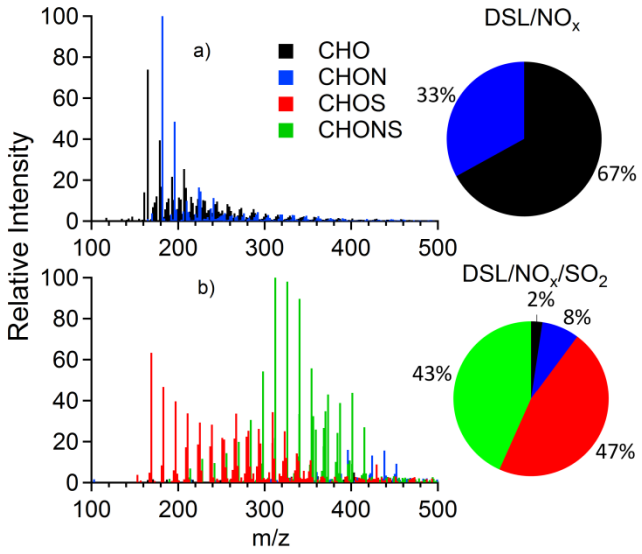

Figure S7. nano-DESI/HRMS spectra, colored by composition, of diesel fuel SOA samples a) 1 (DSL/NOx) and b) 2 (DSL/NOx/SO_2). Pie charts are intensity weighted percent CHONS composition of peaks.

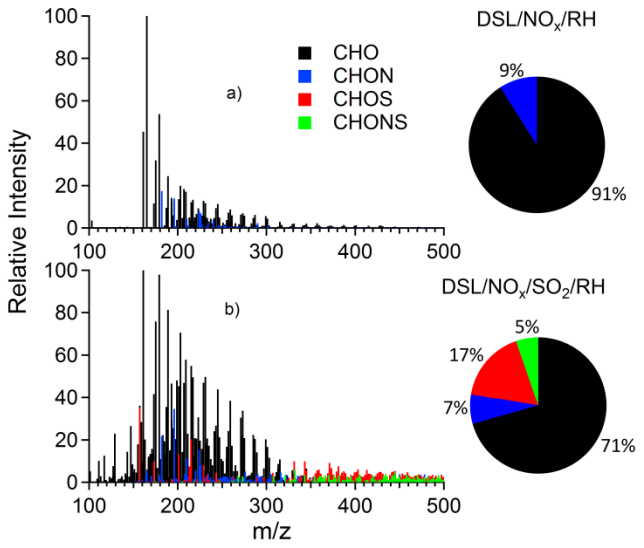

Figure S8. nano-DESI/HRMS spectra, colored by composition, of high humidity diesel fuel SOA samples a) (DSL/NOx/RH) and b) (DSL/NOx/SO_2/RH). Pie charts are intensity weighted percent CHONS composition of peaks.

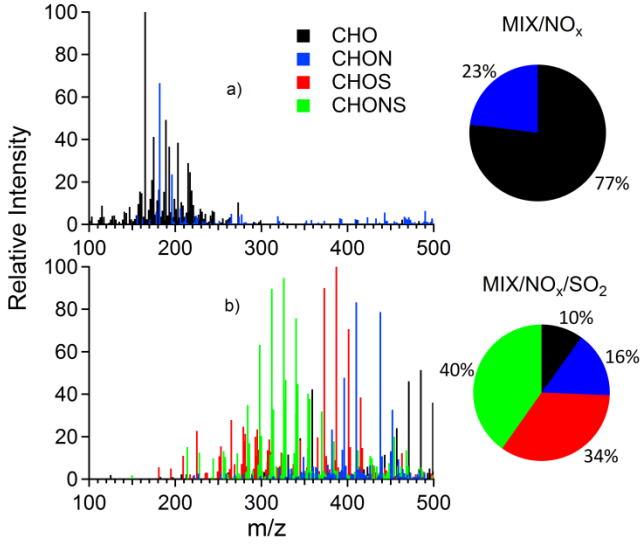

Figure S9. nano-DESI/HRMS spectra, colored by composition, of mixed fuel SOA samples a) 8 (MIX/NOx) and b) 9 (MIX/NOx/SO_2). Pie charts are intensity weighted percent CHONS composition of peaks.

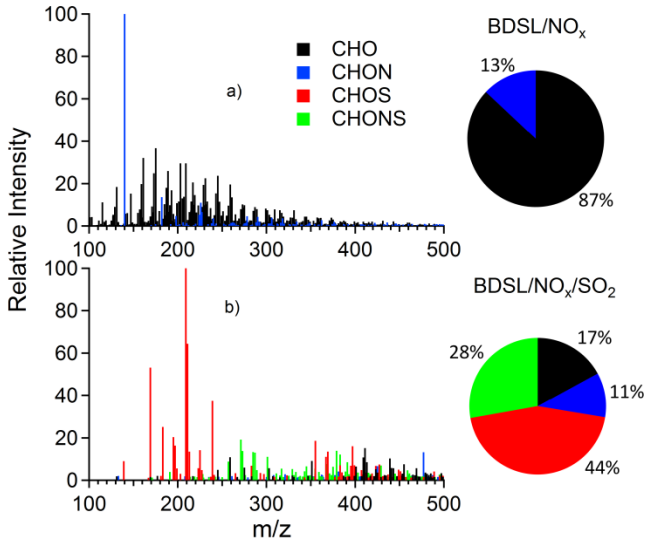

Figure S10. nano-DESI/HRMS spectra, colored by composition, of biodiesel SOA samples a) 6 (BDSL/NOx) and b) 7 (BDSL/NOx/SO_2). Pie charts are intensity weighted percent CHONS composition of peaks.

HR-ToF-AMS Data Analysis and Processing

HR-ToF-AMS data were collecting and analyzed using AMS data analysis software program(s) Squirrel 1.57I and Pika 1.16I. Results for V-mode are reported. For Elemental Analysis involving time-series H/C and O/C ratios, the 2015 "Improved-Ambient" method[11] was used.

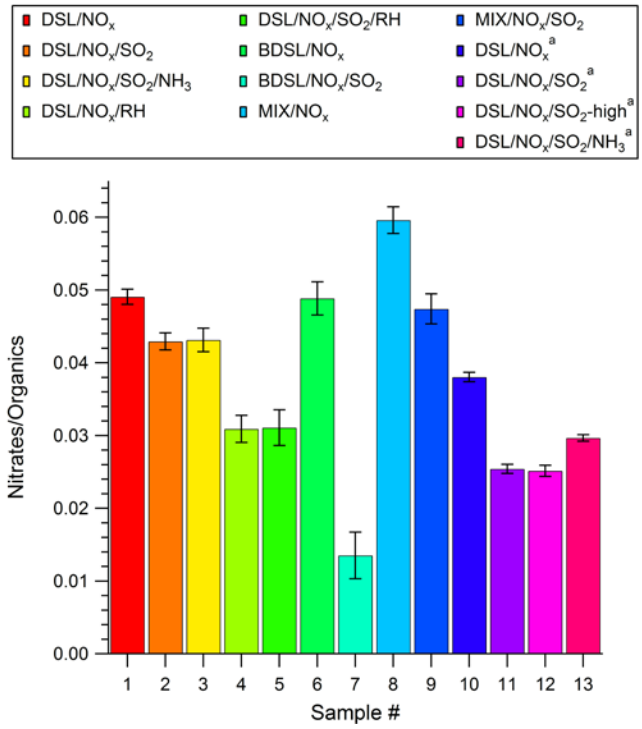

Figure S11. AMS data of SOA samples for particulate nitrates relative to organics. SOA samples are labeled and colored by sample #.

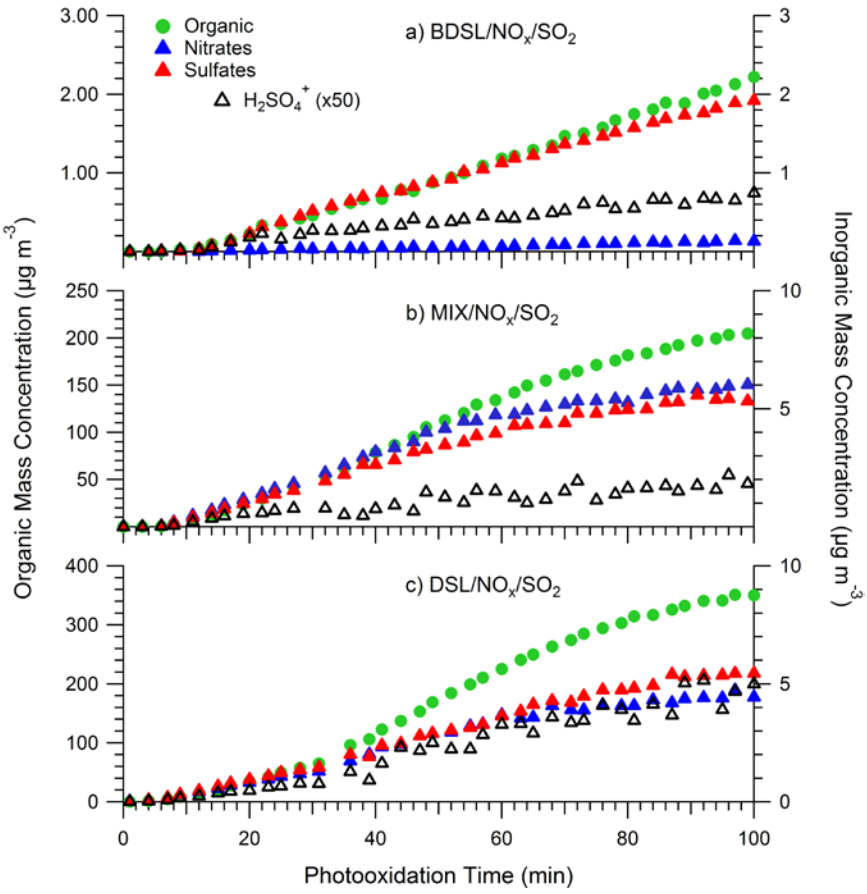

Figure S12. Real-time AMS data during the formation of a) BDSL/NO_x/SO_2, b) MIX/NO_x/SO_2 and, c) DSL/NO_x/SO_2 for $H_2SO_4^+$ (*m/z* 98), total sulphates, total nitrates, and organics.

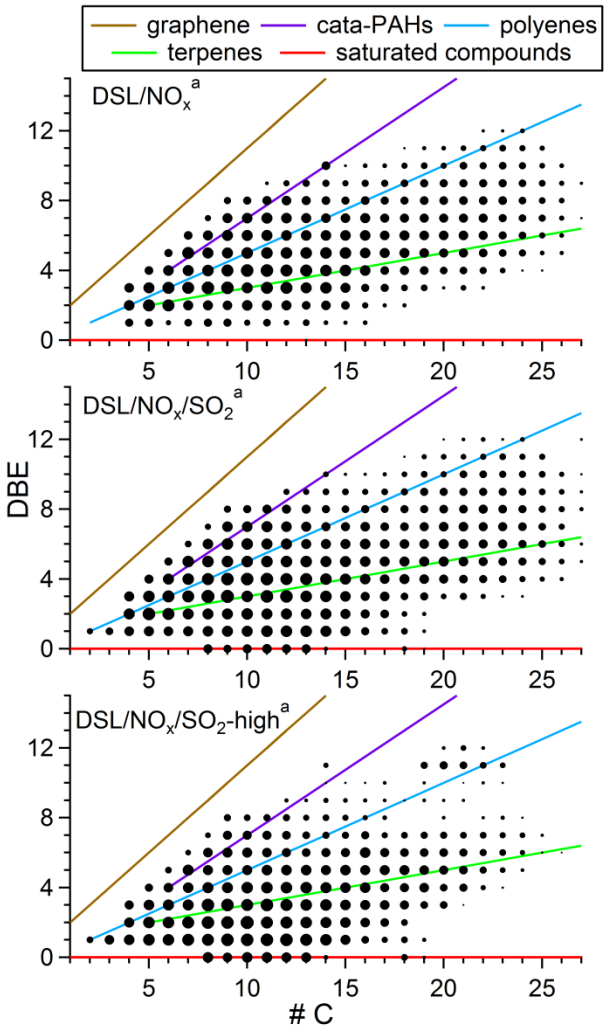

Figure S13. Double bond equivalent (DBE) as a function of carbon number (Cn) for nano-DESI/HRMS diesel fuel SOA samples a) 10, b) 11, and c) 12. The intensities of peaks with a specific Cn and DBE were summed and then the marker size was weighted by this. Trend lines for specific types of species with increasing Cn are plotted in color. Cata-PAHs refer to least compact PAH compounds with 6-membered rings, such as anthracene. The chemical formulas and DBE equations for these are as follows below (Table S4):

Table S4. Definition of species trend lines in Figure S13.

Species	Formula	DBE
graphene	C_n	1 + Cn
cata-PAHs	$C_{2n-6}H_{(C+6)/2}$	0.75·Cn - 0.5
polyenes	C_nH_{n+2}	0.5·Cn
terpenes	$C_{5n}H_{8n}$	0.2·Cn + 1
saturated	$C_{2n}H_{2n+2}$	0

Table S5. Percent CHOS species and percent subsets of CHOS species for each sample. Percent CHOS for each sample are weighted by the sum of the intensity of all peaks within that sample. The subsets of CHOS species are weighted by the sum of the intensity of *only CHOS* peaks for each sample: aliphatic (A), $C_cH_hSO_3$ (B), $C_cH_hSO_4$ (C), and aromatic (D) with an average aromatic index (AI*). An "nd" denotes that peaks of that specific type were not observed.

Sample #	Sample Code	%CHOS	CHOS Subsets				
			%A	%B	%C	%D	<AI*> of D
2	DSL/NO_x/SO_2	47 (92)	30 (37)	1 (nd)	3 (4)	3 (0.2)	0.62 (0.50)
3	DSL/NO_x/SO_2/NH_3	59	42	nd	5	0.3	0.58
5	DSL/NO_x/SO_2/RH	17	0.4	17	20	32	0.57
7	BDSL/NO_x/SO_2	44 (80)	1 (13)	nd (2)	2 (3)	4 (2)	0.72 (0.74)
9	MIX/NO_x/SO_2	34 (80)	25 (37)	29 (nd)	9 (5)	37 (0.3)	0.63 (0.51)
11	DSL/NO_x/SO_2[a]	17 (95)	42 (34)	nd (0.4)	4 (3)	nd (0.1)	nd (0.50)
12	DSL/NO_x/SO_2-high[a]	51 (94)	32 (33)	nd (2)	7 (7)	nd (0.1)	0.61 (0.50)
13	DSL/NO_x/SO_2/NH_3[a]	81 (93)	62 (57)	0.5 (1)	4 (3)	0.5 (0.3)	0.59 (0.53)

[a]Samples sent through a longer denuder train before collection.

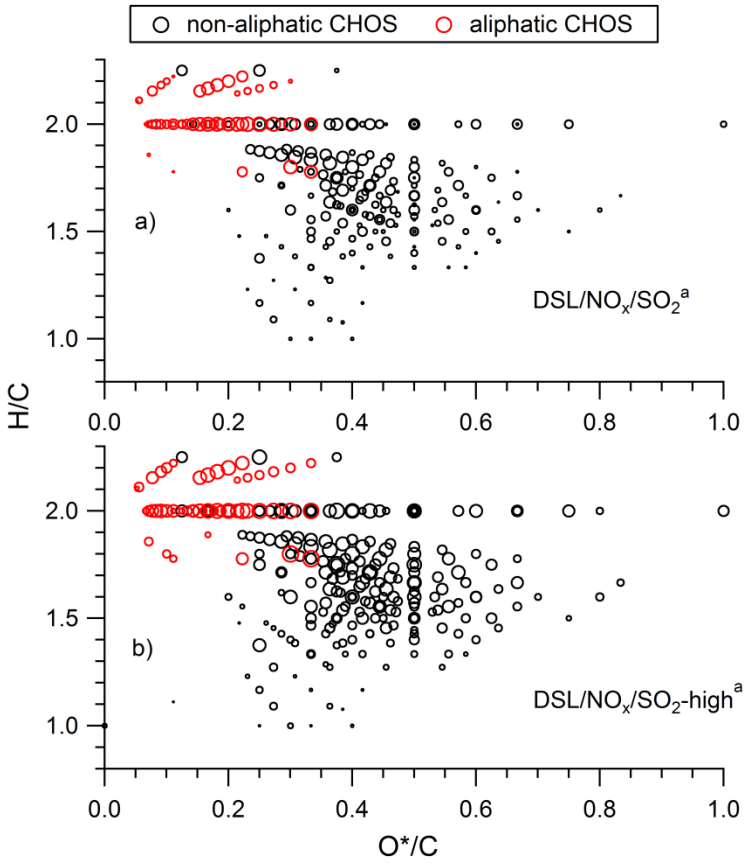

148

149 **Figure S14.** Van Krevelen diagrams of CHOS species (CHO and CHONS not shown) for a)
150 sample 11 (DSL/NOx/SO_{2a}) and b) sample 12 (DSL/NOx/SO_2-$high_a$). O* is the number of
151 oxygen atoms minus 3 to emphasize the degree of oxidation that is not due to the sulfate group
152 addition. Unique aliphatic CHOS species, distinguished by O* < 4 and DBE < 3, are shown in
153 red.

References

(1) Worton, D. R.; Isaacman, G.; Gentner, D. R.; Dallmann, T. R.; Chan, A. W. H.; Ruehl, C.; Kirchstetter, T. W.; Wilson, K. R.; Harley, R. A.; Goldstein, A. H., Lubricating oil dominates primary organic aerosol emissions from motor vehicles. *Environ. Sci. Technol.* 2014, *48* (7), 3698–3706.

(2) Isaacman, G.; Wilson, K. R.; Chan, A. W. H.; Worton, D. R.; Kimmel, J. R.; Nah, T.; Hohaus, T.; Gonin, M.; Kroll, J. H.; Worsnop, D. R.; Goldstein, A. H., Improved resolution of hydrocarbon structures and constitutional isomers in complex mixtures using gas chromatography-vacuum ultraviolet-mass spectrometry. *Anal. Chem.* 2012, *84* (5), 2335–2342.

(3) Chan, A. W. H.; Isaacman, G.; Wilson, K. R.; Worton, D. R.; Ruehl, C. R.; Nah, T.; Gentner, D. R.; Dallmann, T. R.; Kirchstetter, T. W.; Harley, R. A.; Gilman, J. B.; Kuster, W. C.; de Gouw, J. A.; Offenberg, J. H.; Kleindienst, T. E.; Lin, Y. H.; Rubitschun, C. L.; Surratt, J. D.; Hayes, P. L.; Jimenez, J. L.; Goldstein, A. H., Detailed chemical characterization of unresolved complex mixtures in atmospheric organics: Insights into emission sources, atmospheric processing, and secondary organic aerosol formation. *J. Geophys. Res.: Atmospheres* 2013, *118* (12), 6783-6796.

(4) Liu, Y.; Liggio, J.; Staebler, R.; Li, S. M., Reactive uptake of ammonia to secondary organic aerosols: Kinetics of organonitrogen formation. *Atmos. Chem. Phys.* 2015, *15* (23): 13569–13584.

(5) Gentner, D. R.; Isaacman, G.; Worton, D. R.; Chan, A. W. H.; Dallmann, T. R.; Davis, L.; Liu, S.; Day, D. A.; Russell, L. M.; Wilson, K. R.; Weber, R.; Guha, A.; Harley, R. A.; Goldstein, A. H., Elucidating secondary organic aerosol from diesel and gasoline vehicles through detailed characterization of organic carbon emissions. *Proc. Natl. Acad. Sci. U. S. A.* 2012, *109* (45), 18318–18323.

(6) Jathar, S. H.; Donahue, N. M.; Adams, P. J.; Robinson, A. L., Testing secondary organic aerosol models using smog chamber data for complex precursor mixtures: influence of precursor volatility and molecular structure. *Atmos. Chem. Phys.* 2014, *14* (11), 5771–5780.

(7) Pye, H. O. T.; Pouliot, G. A., Modeling the role of alkanes, polycyclic aromatic hydrocarbons, and their oligomers in secondary organic aerosol formation. *Environ. Sci. Technol.* 2012, *46* (11), 6041–6047.

(8) Milazzo, M. F.; Spina, F.; Cavallaro, S.; Bart, J. C. J., Sustainable soy biodiesel. *Renew. Sust. Energ. Rev.* 2013, *27*, 806–852.

(9) Yaakob, Z.; Narayanan, B. N.; Padikkaparambil, S.; Unni, K, S.; Akbar, P, M., A review on the oxidation stability of biodiesel. *Renew. Sust. Energ. Rev.* 2014, *35*, 136–153.

(10) Khoury, R. R.; Ebrahimi, D.; Hejazi, L.; Bucknall, M. P.; Pickford, R.; Brynn Hibbert, D., Degradation of fatty acid methyl esters in biodiesels exposed to sunlight and seawater. *Fuel* 2011, *90* (8), 2677–2683.

(11) Canagaratna, M. R.; Jimenez, J. L.; Kroll, J. H.; Chen, Q.; Kessler, S. H.; Massoli, P.; Hildebrandt Ruiz, L.; Fortner, E.; Williams, L. R.; Wilson, K. R.; Surratt, J. D.; Donahue, N. M.; Jayne, J. T.; Worsnop, D. R., Elemental ratio measurements of organic compounds using aerosol mass spectrometry: characterization, improved calibration, and implications. *Atmos. Chem. Phys.* 2015, *15* (1), 253-272.